Correlations, interactions, and predictability in virus-microbe communities

Ashley R. Coenen[1] and Joshua S. Weitz[2,1,*]

[1]School of Physics, Georgia Institute of Technology, Atlanta, GA, USA
[2]School of Biological Sciences, Georgia Institute of Technology, Atlanta, GA, USA

[*]Corresponding author: jsweitz@gatech.edu

1 Abstract

Microbes are found in high abundances in the environment and in human-associated microbiomes, often exceeding one million per milliliter. Viruses of microbes are found in even higher abundances and are important in shaping microbial populations, communities, and ecosystems. Given the relative specificity of viral infection, it is essential to identify the functional linkages between viruses and their microbial hosts. Multiple approaches have been proposed to infer infection networks from time-series of *in situ* communities, among which correlation-based approaches have emerged as the *de facto* standard. In this work, we evaluate the accuracy of correlation-based inference methods using an *in silico* approach. In doing so, we compare predicted networks to actual networks to assess the self-consistency of correlation-based inference. At odds with assumptions underlying its widespread use, we find that correlation is a poor predictor of interactions in the context of viral infection and lysis of microbial hosts. The failure to predict interactions holds for methods which leverage product-moment, time-lagged, and relative-abundance based correlations. In closing, we discuss alternative inference methods, particularly model-based methods, as a means to infer interactions in complex microbial communities with viruses.

2 Introduction

Viruses of microbes are ubiquitous and highly diverse in marine, soil, and human-associated environments. Viruses interact with their microbial hosts in many ways. For example, they can transfer genes between microbial hosts [1, 2], alter host physiology and metabolism [3, 4], and redirect the flow of organic matter in food webs through cell lysis [5, 6]. Viruses are important parts of microbial communities, and characterizing the interactions between viruses and their microbial hosts is critical for understanding microbial community structure and ecosystem function [5, 7, 8, 9].

A key step in characterizing virus-microbe interactions is determining which viruses can infect which microbes. Viruses are known to be relatively specific but not exclusive in their microbial host range. Individual viruses may infect multiple strains of an isolated microbe or they may infect across genera as part of complex virus-microbe interaction networks [10, 11]. For example, cyanophage can infect both *Prochlorococcus* and *Synechococcus* which are two distinct genera of marine cyanobacteria [12]. However, our knowledge of viral host range remains limited because existing experimental methods for directly testing for viral infection are generally not applicable to an entire *in situ* community. Culture-based methods such as plaque assays are useful for checking for viral infection at the strain level and permit high confidence in their results, but they are not broadly applicable as many viruses and microbes are difficult or currently impossible to isolate and culture [1]. Partially culture-independent methods, such as viral tagging [13, 14] and digital PCR [15], overcome some of these hurdles but only for particular targetable viruses and microbes. Similarly, single-cell genome analysis is able to link individual viruses to microbial hosts [16, 17, 18] but for a relatively small number of cells.

Viral metagenomics offers an alternate route for probing virus-microbe interactions for entire *in situ* communities, bypassing culturing altogether [19, 20, 21]. The viral sequences obtained from metagenomes can be analyzed directly using bioinformatics-based methods to predict microbial hosts [22, 23] although such methods may only be appropriate for a

subset of viruses (DNA viruses but not RNA viruses) and putative hosts (prokaryotes but not eukaryotes). Alternatively, metagenomic sampling of a community *over time* can provide estimates of the changing abundances of viral and microbial populations at high time- and taxonomic- resolution. Once these high-resolution time-series are obtained, they can be used to predict virus-microbe interactions using a variety of statistical and mathematical inference methods (see reviews [24, 25, 26, 27, 28]).

Correlation and correlation-based methods are among the most widely used network inference methods for microbial communities [25]. While this paper focuses on the interactions between microbes and viruses, correlation-based inference methods have been applied more broadly. For example, "extended local similarity analysis" (eLSA) is a correlation-based method which allows for time-lagged correlations [29, 30, 31] and has been used to infer interaction networks in communities of marine bacteria [32, 33]; bacteria and phytoplankton [34, 35]; bacteria and viruses [36]; and bacteria, viruses, and protists [37, 38]. In addition, several correlation-based methods have been developed to address challenges associated with the compositional nature of -omics datasets [39, 25], including "sparse correlations for compositional data" (SparCC) [40].

Regardless of the particular details of these methods, all correlation-based inference operates on the same core assumption: that interacting populations trend together (are correlated) and that non-interacting populations do not trend together (are not correlated). Particular correlation-based methods may relax or augment this assumption. For example, with eLSA the trends may be time-lagged [29, 30, 31]; with simple rank correlations the trends may be non-parametric; and with compositional methods like SparCC the trends may occur between ratios of relative abundances [40]. In communities with only a few populations and simple interactions, population trends may indeed be indicative of ecological mechanism. In these contexts, some correlation-based methods have been shown to recapitulate interactions with limited success [25]. Typically however the challenge of inferring interaction networks applies to diverse communities and complex ecological interactions. Mi-

crobial communities often have dozens, hunderds, or more distinct populations, each of which may interact with many other populations through nonlinear mechanisms such as viral lysis, as well as be influenced by fluctuating abiotic drivers. In these contexts, the relationship between correlation and ecological mechanism is poorly understood. Often correlations do not have a simple mechanistic interpretation, a well-known adage ("correlation does not imply causation") that is often disregarded.

Despite these challenges, correlation-based inference is widely used and rarely verified or benchmarked in advance of its application. Verification of inferred networks is difficult, in part because there is no existing "gold standard" interaction network and, as previously mentioned, direct experimental methods are not widely applicable to *in situ* communities. Therefore, in this work, we take an *in silico* approach to assessing the accuracy of correlation-based inference. To do this, we simulate virus-microbe community dynamics with an interaction network which is prescribed *a priori*. Several existing studies have taken similar *in silico* approaches and found that simple Pearson correlation [41, 39] and several correlation-based methods [25] either fail or are inconsistent in recapitulating interactions networks. However these studies focused on a single *in silico* microbial community [41, 39] or considered only small microbial communities [25]. The goal of this paper is to provide an in-depth assessment of the potential for correlation-based inference given interactions in diverse communities of microbes and viruses. As we show, correlation-based inference fails to recapitulate virus-microbe interactions raising concerns over its use in natural systems.

3 Methods

3.1 Dynamical model of a virus-microbe community

We model the ecological dynamics of a virus-microbe community with a system of nonlinear differential equations:

$$\dot{H}_i = \overbrace{r_i H_i \left(1 - \frac{\sum_{i'}^{N_H} a_{ii'} H_{i'}}{K}\right)}^{\text{microbial growth and competition}} - \overbrace{H_i \sum_{j}^{N_V} M_{ij}\phi_{ij} V_j}^{\text{death by viral lysis}} \tag{1}$$

$$\dot{V}_j = \underbrace{V_j \sum_{i}^{N_H} M_{ij}\phi_{ij}\beta_{ij} H_i}_{\text{release of virions}} - \underbrace{m_j V_j}_{\text{viral decay}} \tag{2}$$

where H_i and V_j refer to the population density of microbial host i and virus j respectively. There are N_H different microbial host populations and N_V different virus populations. For our purposes, a "population" is a group of microbes or viruses with identical life history traits, that is microbes or viruses which occupy the same functional niche.

In the absence of viruses, the microbial hosts undergo logistic growth with growth rates r_i. The microbial hosts have a community-wide carrying capacity K, and they compete with each other for resources both inter- and intra-specifically with competition strength $a_{ii'}$. Each microbial host can be infected and lysed by a subset of viruses determined by the interaction terms M_{ij}. If microbial host i can be infected by virus j, $M_{ij} = 1$; otherwise $M_{ij} = 0$. The collection of all the interaction terms is the interaction network represented by matrix $\mathbf{M}$ of size N_H by N_V. The adsorption rates ϕ_{ij} denote how frequently microbial host i is infected by virus j.

Each virus j's population grows from infecting and lysing their hosts. The rate of virus j's growth is determined by its host-specific adsorption rate ϕ_{ij} and host-specific burst size β_{ij}, which is the number of new virions per infected host cell. The quantity $\tilde{M}_{ij} = M_{ij}\phi_{ij}\beta_{ij}$ is the effective interaction strength between virus j and host i, and the collection of all the

interaction strengths is the weighted interaction network $\tilde{\mathbf{M}}$. Finally, the viruses decay at rates m_j.

3.2 Generating interaction networks and characterizing network structure

Virus-microbe interaction networks, denoted $\mathbf{M}$, are represented as bipartite networks or matrices of size N_H by N_V where N_H is the number of microbial host populations and N_V is the number of virus populations. The element M_{ij} is 1 if microbe population i and virus population j interact and 0 otherwise. In this paper, we consider only square networks ($N = N_H = N_V$) although the analysis is easily extended to rectangular networks. We consider three network sizes $N = 10, 25, 50$.

For each network size N, we generate an ensemble of networks varying in nestedness and modularity (Fig 1). We first generate the maximally nested (Fig 1A) and maximally modular (Fig 1B) networks of size N using the BiMat Matlab package [42]. In order to achieve maximal nestedness and modularity, the network fill F (fraction of interacting pairs) is fixed at $F = 0.55$ for the nested networks and $F = 0.5$ for the modular networks. For the modular networks, the number of modules is set to 2, 5, and 10 for the three network sizes respectively.

To generate networks that vary in nestedness and modularity, we perform the following "rewiring" procedure. Beginning with the maximally nested or maximally modular network, we randomly select an interacting virus-microbe pair ($M_{ij} = 1$) and a non-interacting virus-microbe pair ($M_{i'j'} = 0$) and exchange their values. We do not allow exchanges that would result in an all-zero row or column, as that would isolate the microbe or virus population from the rest of the community. We continue the random selection of pairs without replacement until the desired nestedness or modularity has been achieved. To calculate nestedness and modularity, we use the default algorithms in the BiMat Matlab package. The nestedness metric used is NODF [43], and the algorithm used to calculate modularity is

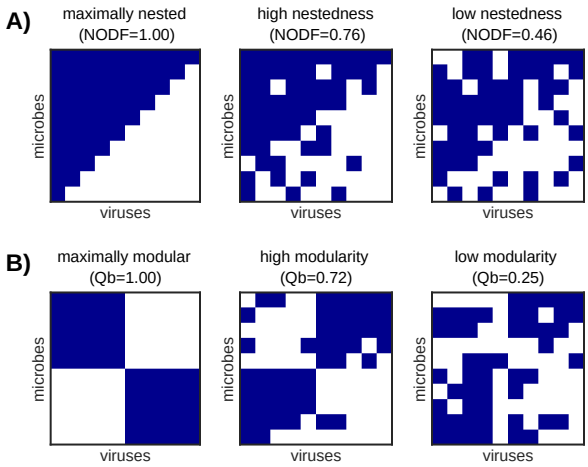

Figure 1: Example interaction networks characterized by A) nestedness and B) modularity. The networks shown here have size $N = 10$ and fill A) $F = 0.55$ and B) $F = 0.5$. Within each network, rows represent microbe populations and columns represent virus populations, while navy squares indicate interaction ($M_{ij} = 1$). Networks were generated according to §3.2. Nestedness (NODF) and modularity (Q_b) were measured with the BiMat package and are arranged in their most nested or most modular forms [42].

AdaptiveBRIM [44]. The modularity is additionally normalized according to a maximum theoretical modularity as detailed in [45].

3.3 Choosing life history traits for coexistence

The life history traits for a given interaction network are chosen to ensure that all microbial host and virus populations can coexist, adapted from [46].

First we sample target fixed point densities H_i^* and V_j^* for each microbial host and virus population. In addition we sample adsorption rates ϕ_{ij} and burst sizes β_{ij}. All of these parameters are chosen by independent random sampling from biologically feasible ranges specified in Table 1. We use a fixed carrying capacity density $K = 10^6$ cells/mL for all parameter sets.

Next we sample microbe-microbe competition terms $a_{ii'}$. We introduce an additional constraint that microbial populations should coexist in the absence of all viruses. We sample target virus-free fixed point densities H_i^{0*} from the range specified in Table 1. According to

	parameter	sampling range	units
H_i^*	host i target steady-state density	$10^3 - 10^4$	cells/mL
V_j^*	virus j target steady-state density	$10^6 - 10^7$	virions/mL
K	community-wide host carrying capacity	10^6	cells/mL
ϕ_{ij}	adsorption rate of virus j into host i	$10^{-7} - 10^{-6}$	mL/ (virion $\cdot$ day)
β_{ij}	burst size of virus j per host i	$10 - 100$	virions/cell
H_i^{0*}	host i target steady-state density in the absence of viruses	$10^3 - 10^6$	cells/mL
$a_{ii'}$	competitive effect of host i' on host i	$0 - 1$	

Table 1: Sampling ranges for parameters in the virus-microbe dynamical model (Eqns 1 and 2).

Eqn 1, coexistence in the virus-free setting is satisfied when

$$K = \sum_{i'}^{N_H} a_{ii'} H_{i'}^{0*} \tag{3}$$

for each microbial host i. We set all intraspecific competition to one ($a_{ii} = 1$) and all interspecific competition to zero ($a_{ii'} = 0$ for $i' \neq i$). Then for each microbial host i we randomly choose an index $k \neq i$ and sample a_{ik} between zero and one. If the updated sum in Eqn 3 does not exceed the carrying capacity K, we repeat for a new index k. Once the carrying capacity is exceeded, we adjust the most recent a_{ik} so that Eqn 3 is satisfied exactly.

Finally, the viral decay rates m_j and host growth rates r_i are computed from the fixed point versions of Eqns 1 and 2:

$$m_j = \sum_{i}^{N_H} M_{ij} \phi_{ij} \beta_{ij} H_i^* \tag{4}$$

$$r_i = \left(\sum_{j}^{N_V} M_{ij} \phi_{ij} V_j^* \right) / \left(1 - \frac{\sum_{i'}^{N_H} a_{ii'} H_{i'}^*}{K} \right) \tag{5}$$

3.4 Simulating and sampling time-series

We use Matlab's native ODE45 function to numerically simulate the virus-microbe dynamical model specified in §3.1 with interaction network and life history traits generated as described in §3.2 and §3.3. We use a relative error tolerance of 10^{-8}. Initial conditions are chosen by perturbing the fixed point densities H_i^* and V_j^* by a multiplicative factor δ where the sign of δ is chosen randomly for each microbial host and virus population.

After simulating virus and microbe time-series, we sample the time-series at regularly spaced sample times (*e.g.* every 2 hours). Therefore, for each virus and each microbe in the community we take S samples at times $t_1, \ldots, t_S$. We use the same sampling frequency and the same S for each inference method, except for time-delayed correlation (see §3.5).

3.5 Standard and time-delayed Pearson correlation networks

We assume S regularly spaced sample times $t_1, \ldots, t_S$ for each host type H_i and each virus type V_j. The samples are log-transformed, that is $h_i(t_k) = \log_{10} H_i(t_k)$ and $v_j(t_k) = \log_{10} V_j(t_k)$ for each sampled time-point t_k. The standard Pearson correlation coefficient between host i and virus j is then

$$r_{ij} = \frac{\sum_{k=1}^{S} \left(h_i(t_k) - \bar{h}_i\right)\left(v_j(t_k) - \bar{v}_j\right)}{\sqrt{\sum_{k=1}^{S} \left(h_i(t_k) - \bar{h}_i\right)^2}\sqrt{\sum_{k=1}^{S} \left(v_j(t_k) - \bar{v}_j\right)^2}} \tag{6}$$

where $\bar{h}_i = \frac{1}{S}\sum_{k=1}^{S} h_i(t_k)$ and $\bar{v}_j = \frac{1}{S}\sum_{k=1}^{S} v_j(t_k)$ are the sample means. The correlation coefficients for all virus-host pairs are represented as a bipartite matrix $\mathbf{R}$ of size $N_H \times N_V$ analogous to the interaction network (see §3.2).

Time-delayed correlations are computed by sampling the virus time-series later in time. Each virus-host pair may have a unique time-delay τ_{ij}. For example, if host i is sampled at times $t_1, \ldots, t_S$ then virus j is sampled at times $t_1 + \tau_{ij}, \ldots, t_S + \tau_{ij}$. We keep the number of samples S fixed, and consequently allow virus j to be sampled beyond the final sample time

t_S of the hosts. The time-delayed Pearson correlation coefficient is

$$r_{ij}^{\tau} = \frac{\sum_{k=1}^{S} \left(h_i(t_k) - \bar{h}_i\right) \left(v_j(t_k + \tau_{ij}) - \bar{v}_j^{\tau_{ij}}\right)}{\sqrt{\sum_{k=1}^{S} \left(h_i(t_k) - \bar{h}_i\right)^2} \sqrt{\sum_{k=1}^{S} \left(v_j(t_k + \tau_{ij}) - \bar{v}_j^{\tau_{ij}}\right)^2}} \tag{7}$$

where $\bar{v}_j^{\tau_{ij}} = \frac{1}{S} \sum_{k=1}^{S} v_j(t_k + \tau_{ij})$ is the mean of the time-delayed virus sample. As before, the correlation coefficients for all virus-host pairs is a bipartite matrix $\mathbf{R}^{\tau}$ of size $N_H \times N_V$.

Pearson correlation coefficients, as specified above, were computed using Matlab's native corr function with type="pearson". Alternate correlation types including Spearman and Kendall are also supported by the corr function and are utilized in the SI.

3.6 eLSA networks

We use samples of all N_H host types and all N_V virus types with S regularly spaced sample times $t_1, \ldots, t_S$ as input for the eLSA computation [29, 30, 31]. We used the lsa-compute.py Python script and set parameters to specify the number of sampled points (spotNum=S), number of replicates (repNum=1), number of bootstraps (b=0), and number of permutations (x=1). All other parameters were left with their default settings including the maximum allowed time delay (delayLimit=3). The lsa-compute.py script computes eLSA scores between all virus-host, host-host, and virus-virus pairs. We selected only the virus-host eLSA scores and arranged them in a bipartite matrix of size $N_H \times N_V$ analogous to the interaction network (see §3.2).

We used a custom Matlab script write_elsa.m to create .csv data files in the format specified by the eLSA documentation. We used a custom bash script elsa_compute_all.sh to run the eLSA analysis on the ensemble of virus-microbe communities. Finally, we used a custom Matlab script read_elsa.m to import the results into Matlab for scoring (see §3.8).

3.7 SparCC networks

SparCC is intended for use with compositional data [40]. Therefore, we normalize the time-series before use with SparCC. Given samples at S regularly spaced sample times $t_1, \ldots, t_S$, we normalize the N_H host types and N_V virus types at each sample time. For example, at sample time t_k, each host type is normalized by

$$\mathcal{N}_{H,k} = \sum_{i=1}^{N_H} H_i(t_k) \tag{8}$$

and each virus type is normalized by

$$\mathcal{N}_{V,k} = \sum_{j=1}^{N_V} V_j(t_k) \tag{9}$$

We use the normalized N_H host and N_V virus samples as input for the SparCC computation using the SparCC.py script. All parameters were left with their default settings.

We used a custom Matlab script write_sparcc.m to create .csv data files in the format specified by the SparCC documentation. We used a custom bash script sparcc_compute_all.sh to run the SparCC analysis on the ensemble of virus-microbe communities. Finally, we used a custom Matlab script read_sparcc.m to import the results into Matlab for scoring (see §3.8).

3.8 Scoring correlation network accuracy

To evaluate how well the Pearson correlation, eLSA, or SparCC (collectively referred to as "correlation") network $\mathbf{R}$ recapitulates the original interaction network $\tilde{\mathbf{M}}$, we compute the receiving operator curve (ROC). First, we binarize the interaction network $\tilde{\mathbf{M}}$ so that it is a boolean network $\mathbf{M}$ of zeros (non-interactions) and ones (interactions). Then we choose a threshold of interaction c between the minimum and maximum attainable values of the correlation network $\mathbf{R}$; for Pearson correlation these are -1 and +1. Correlations in $\mathbf{R}$ that

are greater than or equal to c are categorized as interactions (ones), while those that are less are non-interactions (zeros). The true positive (TP) count is the number of interactions in $\mathbf{M}$ correctly predicted by the thresholded correlation network $\mathbf{R_c}$. The false positive (FP) count is the number of non-interactions in $\mathbf{M}$ incorrectly predicted by $\mathbf{R_c}$. The TP and FP counts are normalized by the number of interactions and non-interactions in $\mathbf{M}$ to obtain the true positive rate (TPR) and false positive rate (FPR). TPR and FPR are computed for all thresholds c to obtain the receiver operator curve (ROC).

The overall "score" of the correlation network $\mathbf{R}$ is the area under the curve (AUC). A perfect prediction results in AUC=1, since for some threshold TPR=1 and FPR=0. Random predictions result in AUC=1/2, since TPR=FPR across all possible thresholds. AUC values which are less than 1/2 indicate a misclassification of "interaction", that is, categorizing interactions and non-interactions in the opposite way would have resulted in a better prediction of $\tilde{\mathbf{M}}$.

4 Results

4.1 Standard Pearson correlation

We calculated the standard Pearson correlation networks for an ensemble *in silico* communities that varied in network size and network structure. For each network size $N = 10, 25, 50$, we generated 20 unique interaction networks. 10 of the networks were generated so that they were distributed along a range of nestedness values, and the other 10 were generated so that they were distributed along a range of modularity values (see §3.2). For each interaction network, life history traits were generated to ensure coexistence using biologically feasible ranges according to §3.3. The mechanistic model for the community dynamics is described in §3.1. Time-series were simulated according to §3.4 with $\delta = 0.3$, that is, the initial conditions were the fixed point values perturbed by 30% (for additional values of δ see Fig S3 in the SI). The time-series were sampled during the transient dynamics to represent *in situ*

communities which are likely perturbed from equilibrium due to changing environmental conditions and intrinsic feedback. We sampled the time-series every 2 hours for 200 hours, that is, we took 100 samples (for additional sample frequencies see Fig S6 in the SI).

For each *in silico* community, we calculated the standard Pearson correlation network as described in §3.5. Two example *in silico* communities of size $N = 10$ are shown in Fig 2 with their simulated time-series, log-transformed samples, and resulting correlation networks. The correlation networks were scored against the original interaction networks by computing AUC as described in §3.8. The procedure for computing AUC is shown in Fig 3 for the two example *in silico* communities.

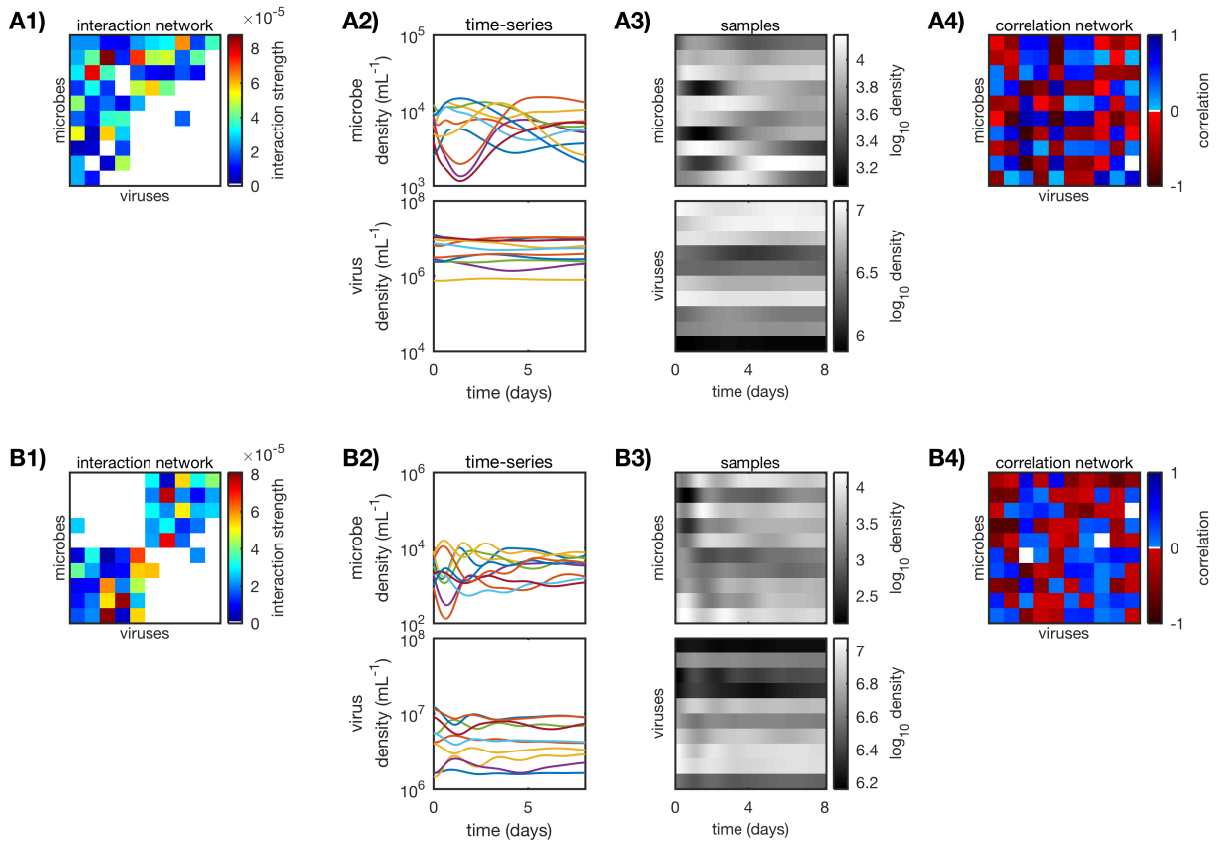

Figure 2: Calculating standard Pearson correlation networks for two *in silico* A) nested and B) modular communities ($N = 10$). A1-B1) Original weighted interaction networks, generated as described in §3.2 and §3.3. A2-B2) Simulated time-series of the virus-microbe dynamical system as described in §3.4 ($\delta = 0.3$). A3-B3) Log-transformed samples, sampled every 2 hours for 200 hours from the simulated time-series. A4-B4) Pearson correlation networks, calculated from log-transformed samples as described in §3.5.

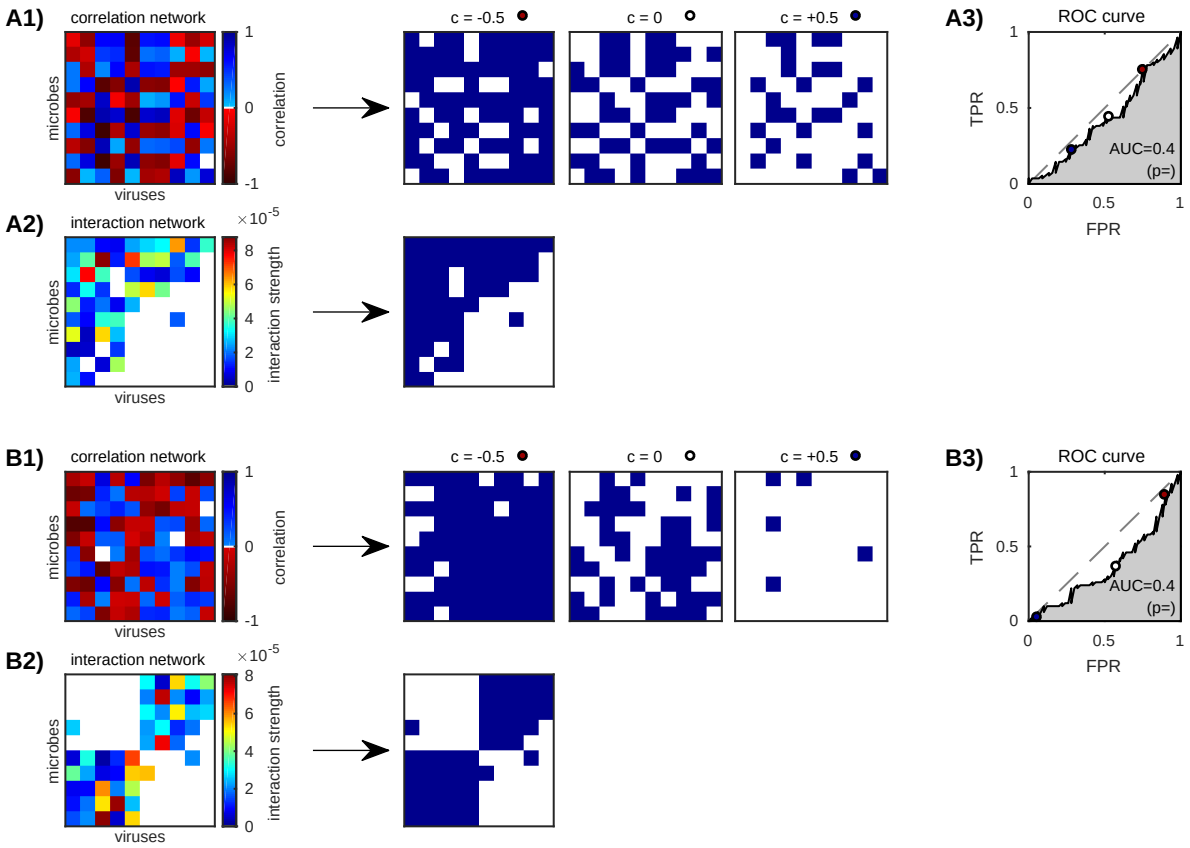

Figure 3: Scoring correlation network accuracy of the two *in silico* A) nested and B) modular communities ($N = 10$, see Fig 2) as described in §3.8. A1-B1) Correlation networks are binarized according to thresholds c between -1 and $+1$, three of which are shown here ($c = -0.5, 0,$ and 0.5). A2-B2) Original interaction networks are also binarized. A3-B3) True positive rate (TPR) versus false positive rate (FPR) of the binarized correlation networks for each threshold c. Three example thresholds ($c = -0.5, 0,$ and 0.5) are marked (red, white, and blue circles). The "non-discrimination" line (grey dashed) is where TPR = FPR. The AUC or area under the ROC curve is a measure of relative TPR to FPR over all thresholds; AUC = 1 is a perfect result. Distributions for the reported p-values are shown in the SI.

AUC values for all *in silico* communities are shown in Fig 4. Across varying network size and network structure, AUC is approximately 1/2 implying that standard Pearson correlation networks lack predictive power. Similar results were found when varying the initial condition perturbation δ (Fig S3) and the sampling frequency (Fig S6). There are some cases for the smaller networks ($N = 10$) where AUC does deviate from 1/2 although these deviations are small ($\approx \pm 10\%$). Interestingly these deviations tend to be negative indicating a misclassification of the interaction condition, that is, negative correlations are slightly better

predictors of interaction than positive correlations. Overall however, the deviations disappear for larger networks ($N = 50$) implying that they are exceptions rather than the norm. We completed identical analyses for additional correlation metrics in particular Spearman correlation and Kendall correlation (see Fig S1 in SI). We found similar results reinforcing our conclusion that simple correlations between time-series are poor predictors of the underlying interaction network.

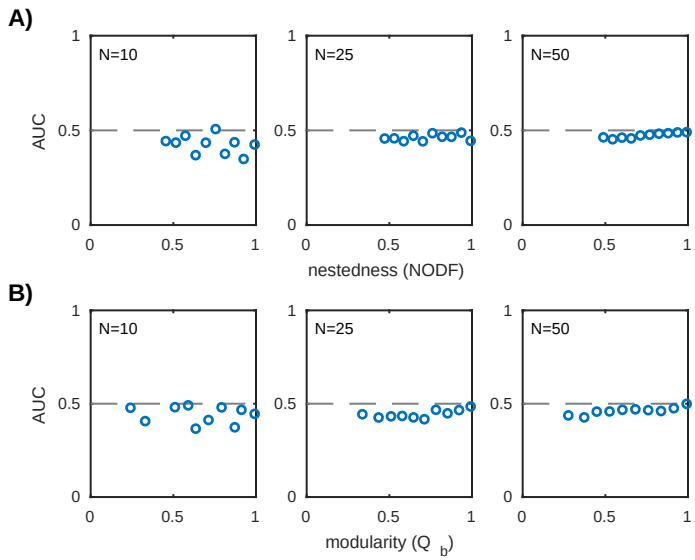

Figure 4: AUC values for standard Pearson correlation for the ensemble of A) nested and B) modular communities over three network sizes $N = 10, 25, 50$ (20 communities for each network size). AUC is computed as described in §3.8. Each plotted point corresponds to a unique *in silico* community. Dashed line marks AUC=1/2 and implies the predicted network did no better than random guessing.

4.2 Time-delayed Pearson correlation

Given the results of the previous section §4.1 – that standard correlations do not recapitulate interactions – we computed time-delayed correlation networks for the same ensemble of *in silico* communities. The addition of time-delays to standard correlation approaches is motivated by a large body of theoretical work on predator-prey dynamics, where both predator and prey populations oscillate but with a phase delay between them [47]. Similar results hold

for the phase delay in simple phage-bacteria dynamics [48]. Time-delayed correlations are the basis of several existing correlation-based inference methods including eLSA [29, 30, 31].

For this analysis, we used the same ensemble of *in silico* communities (network sizes $N = 10, 25, 50$ of varying nestedness and modularity), simulated time-series ($\delta = 0.3$; see Fig S4 in SI), and sample frequency (2 hours; see Fig S7 in SI) as before (see §4.1 for time-series). We calculated the time-delayed Pearson correlation networks as described in §3.5, where for each virus-host pair the virus time-series is sampled later in time by some delay amount τ_{ij} relative to the host time-series (for Spearman and Kendall correlation, see Fig S2 in SI). Each delay is chosen such that the absolute value of the correlation for the virus-host pair is maximized. Since the optimal time-delay is not known in advance, delays between $0 < \tau_{ij} < t_S/2$, (0 hours and $t_S/2 = 100$ hours) were considered. The number of samples used to compute each correlation coefficient was kept fixed at $S = 100$ (sample duration 200 hours). Time-delayed Pearson correlation networks for the two example *in silico* communities of size $N = 10$ are shown in Fig 5A-B. AUC was computed as described in §3.8.

AUC values for all *in silico* communities are shown in Fig 5C. For the small networks ($N = 10$) there are a few particular networks which have AUC scores greater than 1/2. For the remaining small networks and the large networks ($N = 25, 50$), AUC $\approx 1/2$ implying time-delayed Pearson correlation lacks predictive power for these networks. Similar results were found for alternate correlation metrics (Spearman and Kendall; Fig S2), initial condition perturbations δ (Fig S4), and sampling frequencies (Fig S7). Because AUC deviates from 1/2 for only a few small networks and disappears for large networks, it should be considered an exceptional result rather than the norm for time-delayed Pearson correlation.

4.3 Correlation-based methods eLSA and SparCC

We performed a similar *in silico* analysis using eLSA [29, 30, 31] and SparCC [40], two established correlation-based inference methods which are widely used with *in situ* time-

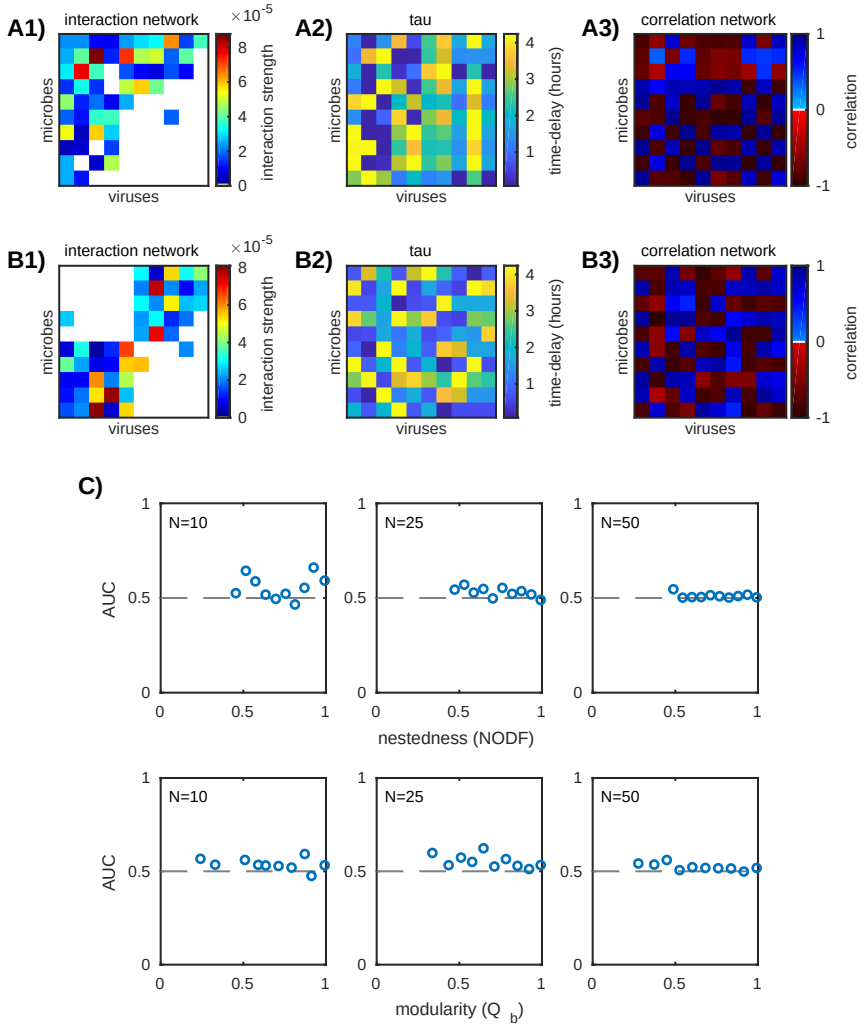

Figure 5: Performance of time-delayed Pearson correlation. A1-B1) Two example *in silico* interaction networks ($N = 10$). A2-B2) Time-delays τ_{ij} for each virus-host pair, chosen so that the absolute value of the correlation is maximized. A3-B3) Time-delayed Pearson correlation networks calculated as described in §3.5. C) AUC values for the ensemble of nested (top row) and modular (bottom row) communities over three network sizes $N = 10, 25, 50$ (20 communities for each network size). Each plotted point corresponds to a unique *in silico* community. Dashed line marks AUC=1/2 and implies the predicted network did no better than random guessing.

series data. We used the same ensemble of *in silico* communities as before (network sizes $N = 10, 25, 50$ of varying nestedness and modularity), along with the simulated time-series ($\delta = 0.3$; see Fig S5), sample frequency (2 hours; see Fig S8) and sample duration (200 hours). We implemented eLSA and SparCC as described in §3.6 and §3.7 respectively. eLSA and SparCC predicted networks for the two example *in silico* communities of size $N = 10$

are shown in Fig 6A-B. AUC was computed as before and as described in §3.8.

AUC values for all *in silico* communities are shown in Fig 6C. We see the same trends as with standard correlation and time-delayed correlation (see Figs 4 and 5). Similar results hold for varying values of the initial condition perturbation δ (Fig S5) and sampling frequency (Fig S8). For small networks ($N = 10$), there are a few AUC scores which deviate weakly from 1/2 ($\approx \pm 10\%$). Interestingly, AUC scores for eLSA tend to be negative, implying a misclassification of interaction. AUC converges to 1/2 as network size increases ($N = 25, 50$) indicating that the AUC scores for small networks may themselves be spurious.

5 Discussion

Using *in silico* virus-microbe community dynamics, we calculated correlation networks among viral and microbial population time-series samples. We tested the accuracy of several different types of correlation and time-delayed correlation (Pearson, Spearman, and Kendall) and existing correlation-based inference methods (eLSA and SparCC). The correlation networks for all of these implementations failed to effectively predict the original interaction networks, as quantified by the AUC score. Failure persisted across variation in network structure, network size, initial condition perturbation amount, and sampling frequency. We therefore conclude these correlation-based inference methods do not meaningfully predict interactions given this mechanistic model of virus-microbe community dynamics.

Earlier, we stated the core assumption of correlation-based inference: that interacting populations are correlated and that non-interacting populations are not correlated. While this core assumption sometimes holds in small communities with simple interaction mechanisms [25], we find it does not necessarily hold in more complex communities. In particular, we considered communities with microbes and viruses that interacted through a nonlinear mechanism (infection and lysis) across a spectrum of network sizes and network structure. We found that correlation-based inference performed poorly given variation in these network

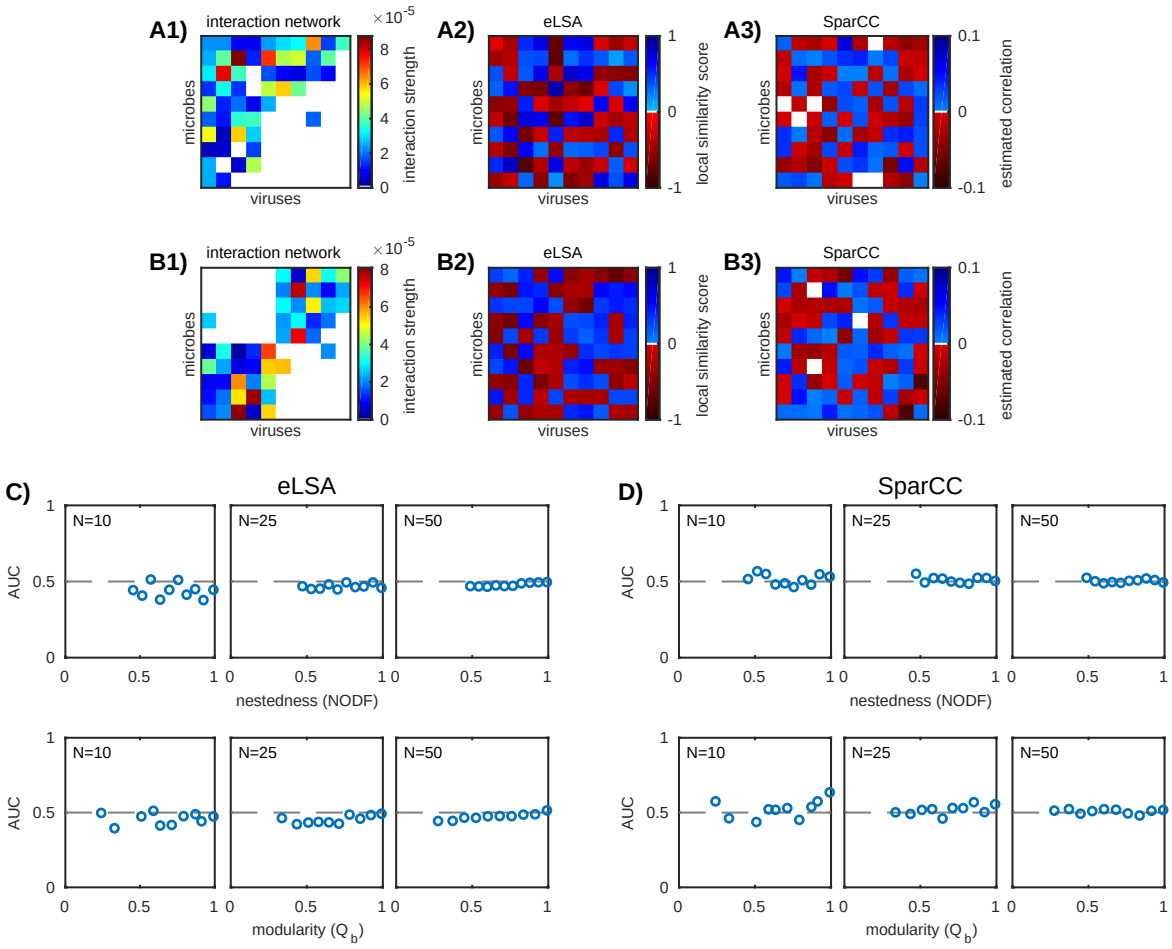

Figure 6: Performance of correlation-based inference methods eLSA and SparCC. A1-B1) Two example *in silico* interaction networks ($N = 10$). A2-B2) eLSA predicted network computed as described in §3.6. A3-B3) SparCC predicted network computed as described in §3.7 (color bar adjusted for visibility). C-D) AUC values for the ensemble of nested (top row) and modular (bottom row) communities over three network sizes $N = 10, 25, 50$ (20 communities for each network size). Each plotted point corresponds to a unique *in silico* community. Dashed line marks AUC=1/2 and implies the predicted network did no better than random guessing.

properties, but that there was greater variation in performance for small networks. Because this variation is relatively small and disappears for larger networks, successful predictions for small networks may themselves be spurious. Namely, for a small networks, there is a greater probability of randomly guessing the interactions correctly because the space of possible networks is smaller.

Our results raise concerns about the use of correlation-based methods on *in situ* datasets,

since a typical community under consideration will have dozens or more interacting strains and therefore will not be in the low diversity regime explored by [25]. Additional challenges such as external environmental drivers, measurement noise, and system stochasticity must also be carefully considered before applying correlation-based methods to *in situ* datasets. In light of the poor performance of correlation-based methods, we advocate for increased studies of model-based inference. Model-based inference methods operate by first assuming an underlying dynamical model for the community – unlike correlation-based methods, which assume that similar trends in population indicate interaction. Model-based inference has the potential to be tailored to complex communities and environments while leveraging existing knowledge about ecological mechanisms. After assuming a dynamical model, model-based inference methods use a variety of optimization and regression techniques predict an interaction network which best describes the observed population time-series. Given favorable results of *in silico* benchmarking of model-based inference methods [41, 39, 49, 50, 51, 52], it will be important to investigate the efficacy of model-based inference methods for microbial communities both *in silico* and in practice.

6 Acknowledgments

We are grateful to Ben Bolduc, Stephen Beckett, and two anonymous reviewers for helpful comments and feedback. We thank both Yu-Hui Lin and David Demory for reviewing the code used in the analysis. This work was supported by the Simons Foundation (SCOPE award ID 329108, J.S.W.).

7 Availability of data and materials

Analysis was primarily performed in Matlab. All Matlab scripts, Matlab data files, and custom bash scripts for implementing eLSA and SparCC are publicly available on GitHub (`https://github.com/WeitzGroup/correlation_based_inference`) and archived on Zen-

odo (DOI 10.5281/zenodo.844918). The BiMat Matlab package [42] used for characterizing bipartite networks is available on GitHub (`https://github.com/cesar7f/BiMat`). The eLSA Python package [29, 30, 31] is available on Bitbucket (`https://bitbucket.org/charade/elsa/wiki/Home`). The SparCC Python package [40] is available on Bitbucket (`https://bitbucket.org/yonatanf/sparcc`).

References

[1] F. Rohwer and R. V. Thurber, "Viruses manipulate the marine environment," *Nature*, vol. 459, no. 7244, pp. 207–12, 2009.

[2] L. D. McDaniel, E. Young, J. Delaney, F. Ruhnau, K. B. Ritchie, and J. H. Paul, "High frequency of horizontal gene transfer in the oceans," *Science*, vol. 330, no. 6000, p. 50, 2010.

[3] K. D. Bidle and A. Vardi, "A chemical arms race at sea mediates algal host-virus interactions," *Curr Opin Microbiol*, vol. 14, no. 4, pp. 449–57, 2011.

[4] D. Lindell, M. B. Sullivan, Z. I. Johnson, A. C. Tolonen, F. Rohwer, and S. W. Chisholm, "Transfer of photosynthesis genes to and from prochlorococcus viruses," *Proc Natl Acad Sci U S A*, vol. 101, no. 30, pp. 11013–8, 2004.

[5] J. S. Weitz and S. W. Wilhelm, "Ocean viruses and their effects on microbial communities and biogeochemical cycles," *F1000 Biol Rep*, vol. 4, p. 17, 2012.

[6] C. A. Suttle, "Viruses in the sea," *Nature*, vol. 437, no. 7057, pp. 356–61, 2005.

[7] J. R. Brum, J. C. Ignacio-Espinoza, S. Roux, G. Doulcier, S. G. Acinas, A. Alberti, S. Chaffron, C. Cruaud, C. de Vargas, J. M. Gasol, G. Gorsky, A. C. Gregory, L. Guidi, P. Hingamp, D. Iudicone, F. Not, H. Ogata, S. Pesant, B. T. Poulos, S. M. Schwenck, S. Speich, C. Dimier, S. Kandels-Lewis, M. Picheral, S. Searson, , P. Bork, C. Bowler, S. Sunagawa, P. Wincker, E. Karsenti, and M. B. Sullivan, "Patterns and ecological drivers of ocean viral communities," *Science*, vol. 348, no. 6237, 2015.

[8] M. Breitbart, "Marine viruses: Truth or dare," *Annual Review of Marine Science*, 2012.

[9] C. Brussaard, "Viral control of phytoplankton populations – a review," *Journal of Eukaryotic Microbiology*, 2005.

[10] J. S. Weitz, T. Poisot, J. R. Meyer, C. O. Flores, S. Valverde, M. B. Sullivan, and M. E. Hochberg, "Phage-bacteria infection networks," *Trends Microbiol*, vol. 21, no. 2, pp. 82–91, 2013.

[11] C. O. Flores, S. Valverde, and J. S. Weitz, "Multi-scale structure and geographic drivers of cross-infection within marine bacteria and phages," *ISME J*, vol. 7, no. 3, pp. 520–32, 2013.

[12] M. B. Sullivan, J. B. Waterbury, and S. W. Chisholm, "Cyanophages infecting the oceanic cyanobacterium prochlorococcus," *Nature*, vol. 424, no. 6952, pp. 1047–51, 2003.

[13] L. Deng, A. Gregory, S. Yilmaz, B. T. Poulos, P. Hugenholtz, and M. B. Sullivan, "Contrasting life strategies of viruses that infect photo- and heterotrophic bacteria, as revealed by viral tagging," *MBio*, vol. 3, no. 6, 2012.

[14] L. Deng, J. C. Ignacio-Espinoza, A. C. Gregory, B. T. Poulos, J. S. Weitz, P. Hugenholtz, and M. B. Sullivan, "Viral tagging reveals discrete populations in synechococcus viral genome sequence space," *Nature*, vol. 513, no. 7517, pp. 242–5, 2014.

[15] A. D. Tadmor, E. A. Ottesen, J. R. Leadbetter, and R. Phillips, "Probing individual environmental bacteria for viruses by using microfluidic digital pcr," *Science*, vol. 333, no. 6038, pp. 58–62, 2011.

[16] S. Roux, A. K. Hawley, M. T. Beltran, M. Scofield, P. Schwientek, R. Stepanauskas, T. Woyke, S. J. Hallam, and M. B. Sullivan, "Ecology and evolution of viruses infecting uncultivated sup05 bacteria as revealed by single-cell- and meta-genomics," *eLIFE*, 2014.

[17] J. M. Labonte, B. K. Swan, B. Poulos, H. Luo, S. Koren, S. J. Hallam, M. B. Sullivan, T. Woyke, K. E. Wommack, and R. Stepanauskas, "Single-cell genomics-based analysis of virus-host interactions in marine surface bacterioplankton," *ISME J*, 2015.

[18] J. H. Munson-McGee, S. Peng, S. Dewerff, R. Stepanauskas, R. J. Whitaker, J. S. Weitz, and M. J. Young, "A virus or more in (nearly) every cell: ubiquitous networks of virus-host interactions in extreme environments," *ISME J*, 2018.

[19] M. Breitbart, P. Salamon, B. Andresen, J. M. Mahaffy, A. M. Segall, D. Mead, F. Azam, and F. Rohwer, "Genomic analysis of uncultured marine viral communities," *Proc Natl Acad Sci U S A*, vol. 99, no. 22, pp. 14250–5, 2002.

[20] R. A. Edwards and F. Rohwer, "Viral metagenomics," *Nat Rev Microbiol*, vol. 3, no. 6, pp. 504–10, 2005.

[21] M. R. Clokie, A. D. Millard, A. V. Letarov, and S. Heaphy, "Phages in nature," *Bacteriophage*, vol. 1, no. 1, pp. 31–45, 2011.

[22] S. Roux, F. Enault, B. L. Hurwitz, and M. B. Sullivan, "Virsorter: mining viral signal from microbial genomic data," *PeerJ*, 2015.

[23] R. A. Edwards, K. McNair, K. Faust, J. Raes, and B. E. Dutilh, "Computational approaches to predict bacteriophage-host relationships," *FEMS Microbiology Reviews*, 2015.

[24] M. Layeghifard, D. M. Hwang, and D. S. Guttman, "Disentangling interactions in the microbiome: A network perspective," *Trends Microbiol*, vol. 25, no. 3, pp. 217–228, 2017.

[25] S. Weiss, W. Van Treuren, C. Lozupone, K. Faust, J. Friedman, Y. Deng, L. C. Xia, Z. Z. Xu, L. Ursell, E. J. Alm, A. Birmingham, J. A. Cram, J. A. Fuhrman, J. Raes, F. Sun, J. Zhou, and R. Knight, "Correlation detection strategies in microbial data sets vary widely in sensitivity and precision," *ISME J*, vol. 10, no. 7, pp. 1669–81, 2016.

[26] K. Faust, L. Lahti, D. Gonze, W. M. de Vos, and J. Raes, "Metagenomics meets time series analysis: unraveling microbial community dynamics," *Curr Opin Microbiol*, vol. 25, pp. 56–66, 2015.

[27] K. Faust and J. Raes, "Microbial interactions: from networks to models," *Nat Rev Microbiol*, vol. 10, no. 8, pp. 538–50, 2012.

[28] J. A. Fuhrman, "Microbial community structure and its functional implications," *Nature*, vol. 459, no. 7244, pp. 193–9, 2009.

[29] Q. Ruan, D. Dutta, M. S. Schwalbach, J. A. Steele, J. A. Fuhrman, and F. Sun, "Local similarity analysis reveals unique associations among marine bacterioplankton species and environmental factors," *Bioinformatics*, vol. 22, no. 20, pp. 2532–8, 2006.

[30] L. C. Xia, J. A. Steele, J. A. Cram, Z. G. Cardon, S. L. Simmons, J. J. Vallino, J. A. Fuhrman, and F. Sun, "Extended local similarity analysis (elsa) of microbial community and other time series data with replicates," *BMC Syst Biol*, vol. 5 Suppl 2, p. S15, 2011.

[31] L. C. Xia, D. Ai, J. Cram, J. A. Fuhrman, and F. Sun, "Efficient statistical significance approximation for local similarity analysis of high-throughput time series data," *Bioinformatics*, vol. 29, no. 2, pp. 230–7, 2013.

[32] C. E. Chow, R. Sachdeva, J. A. Cram, J. A. Steele, D. M. Needham, A. Patel, A. E. Parada, and J. A. Fuhrman, "Temporal variability and coherence of euphotic zone bacterial communities over a decade in the southern california bight," *ISME J*, vol. 7, no. 12, pp. 2259–73, 2013.

[33] J. A. Gilbert, J. A. Steele, J. G. Caporaso, L. Steinbruck, J. Reeder, B. Temperton, S. Huse, A. C. McHardy, R. Knight, I. Joint, P. Somerfield, J. A. Fuhrman, and D. Field, "Defining seasonal marine microbial community dynamics," *ISME J*, vol. 6, no. 2, pp. 298–308, 2012.

[34] L. Liu, J. Yang, H. Lv, and Z. Yu, "Synchronous dynamics and correlations between bacteria and phytoplankton in a subtropical drinking water reservoir," *FEMS Microbiol Ecol*, vol. 90, no. 1, pp. 126–38, 2014.

[35] S. F. Paver, K. R. Hayek, K. A. Gano, J. R. Fagen, C. T. Brown, A. G. Davis-Richardson, D. B. Crabb, R. Rosario-Passapera, A. Giongo, E. W. Triplett, and A. D. Kent, "Interactions between specific phytoplankton and bacteria affect lake bacterial community succession," *Environmental Microbiology*, vol. 15, no. 9, pp. 2489–2504, 2013.

[36] D. M. Needham, C. E. Chow, J. A. Cram, R. Sachdeva, A. Parada, and J. A. Fuhrman, "Short-term observations of marine bacterial and viral communities: patterns, connections and resilience," *ISME J*, vol. 7, no. 7, pp. 1274–85, 2013.

[37] C. E. Chow, D. Y. Kim, R. Sachdeva, D. A. Caron, and J. A. Fuhrman, "Top-down controls on bacterial community structure: microbial network analysis of bacteria, t4-like viruses and protists," *ISME J*, vol. 8, no. 4, pp. 816–29, 2014.

[38] J. A. Steele, P. D. Countway, L. Xia, P. D. Vigil, J. M. Beman, D. Y. Kim, C. E. Chow, R. Sachdeva, A. C. Jones, M. S. Schwalbach, J. M. Rose, I. Hewson, A. Patel, F. Sun, D. A. Caron, and J. A. Fuhrman, "Marine bacterial, archaeal and protistan association networks reveal ecological linkages," *ISME J*, vol. 5, no. 9, pp. 1414–25, 2011.

[39] Z. D. Kurtz, C. L. Muller, E. R. Miraldi, D. R. Littman, M. J. Blaser, and R. A. Bonneau, "Sparse and compositionally robust inference of microbial ecological networks," *PLoS Comput Biol*, vol. 11, no. 5, p. e1004226, 2015.

[40] J. Friedman and E. J. Alm, "Inferring correlation networks from genomic survey data," *PLoS Comput Biol*, vol. 8, no. 9, p. e1002687, 2012.

[41] C. K. Fisher and P. Mehta, "Identifying keystone species in the human gut microbiome from metagenomic timeseries using sparse linear regression," *PLoS One*, vol. 9, no. 7, p. e102451, 2014.

[42] C. O. Flores, T. Poisot, S. Valverde, and J. S. Weitz, "Bimat: a matlab package to facilitate the analysis of bipartite networks," *Methods in Ecology and Evolution*, vol. 7, no. 1, pp. 127–132, 2016.

[43] M. Almeida-Neto, P. Guimares, P. R. Guimares, R. D. Loyola, and W. Ulrich, "A consistent metric for nestedness analysis in ecological systems: reconciling concept and measurement," *Oikos*, vol. 117, no. 8, pp. 1227–1239, 2008.

[44] M. J. Barber, "Modularity and community detection in bipartite networks," *Phys. Rev. E*, vol. 76, p. 066102, Dec 2007.

[45] S. J. Beckett, "Improved community detection in weighted bipartite networks," *R Soc Open Sci*, vol. 3, no. 1, p. 140536, 2016.

[46] L. F. Jover, M. H. Cortez, and J. S. Weitz, "Mechanisms of multi-strain coexistence in host-phage systems with nested infection networks," *J Theor Biol*, vol. 332, pp. 65–77, 2013.

[47] M. Rosenzweig and R. H. MacArthur, "Graphical representation and stability conditions of predator-prey interactions," vol. 97, pp. 209–223, 01 1963.

[48] J. S. Weitz, *Quantitative Viral Ecology*. Princeton University Press, 2015.

[49] R. R. Stein, V. Bucci, N. C. Toussaint, C. G. Buffie, G. Ratsch, E. G. Pamer, C. Sander, and J. B. Xavier, "Ecological modeling from time-series inference: insight into dynamics and stability of intestinal microbiota," *PLoS Comput Biol*, vol. 9, no. 12, p. e1003388, 2013.

[50] L. F. Jover, J. Romberg, and J. S. Weitz, "Inferring phage-bacteria infection networks from time-series data," *R Soc Open Sci*, vol. 3, no. 11, p. 160654, 2016.

[51] P. Dam, L. L. Fonseca, K. T. Konstantinidis, and E. O. Voit, "Dynamic models of the complex microbial metapopulation of lake mendota," *NPJ Syst Biol Appl*, vol. 2, p. 16007, 2016.

[52] S. Marino, N. T. Baxter, G. B. Huffnagle, J. F. Petrosino, and P. D. Schloss, "Mathematical modeling of primary succession of murine intestinal microbiota," *Proc Natl Acad Sci U S A*, vol. 111, no. 1, pp. 439–44, 2014.